

From quantum Rabi model to Jaynes-Cummings model: symmetry-breaking quantum phase transitions, topological phase transitions and multicriticalities

Zu-Jian Ying*

School of Physical Science and Technology, Lanzhou University, Lanzhou 730000, China

We study the ground state (GS) and excitation gap of anisotropic quantum Rabi model (QRM) which connects the fundamental QRM and the Jaynes-Cummings model (JCM). While the GS has a second-order quantum phase transition (QPT) in the low frequency limit, turning on finite frequencies we shed a novel light on the phase diagram to illuminate a fine structure of first-order transition series. We find the QPT is accompanied with a hidden symmetry breaking, whereas the emerging series transitions are topological transitions without symmetry breaking. The topological structure of the wave function provides a novel universality classification in bridging the QRM and the JCM. We show that the conventionally established triple point is actually a quintuple or sextuple point and following the penta-/hexa-criticality emerge a series of tetra-criticalities.

PACS numbers:

Introduction.—In the past decade the frontiers of quantum physics have witnessed both experimental [1, 2] and theoretical [3, 4] advances in the study of the light-matter interaction. The experimental access to ultrastrong coupling regime [1, 5–14] has brought a rich phenomenology unexpected in weak couplings [1, 2]. On the other hand, the recent milestone theoretical work of revealing the Braak integrability [3] has attracted tremendous attention on the quantum Rabi model (QRM) and its extensions [4, 15–44]. The QRM [45] and the Jaynes-Cummings model (JCM) [46] are the most fundamental models for the light-matter interaction. They are also fundamental building blocks for quantum information and quantum computation [1, 47] and closely connected to models in condensed matter [2].

The essential difference of the QRM and the JCM lies in the counter-rotating interaction. Both experimental measurements [5, 48, 49] and theoretical studies [22, 25] have raised the concern on the role of the counter-rotating interaction, a full understanding of which is one of the central topics in investigations of light-matter interaction. The coupling anisotropy tunes the strength of the counter-rotating interaction, thus the anisotropic QRM is the bridge of the two fundamental models. The anisotropic QRM is integrable [22] and interestingly the model exhibits a few-body quantum phase transition which can be connected to the many-body and thermodynamical cases via the scaling of critical components [25].

Generally the study of phase transitions has stimulated the developments of theoretical physics in deepening the understanding of nature. The traditional Landau theory [50] made a breakthrough to realize that different phases correspond to the realization of different symmetries and a phase transition undergoes a symmetry breaking. In the last decades, a new class of phases was discovered coined the term "topological phases" [51–55]. The occurrence of topological phase transition requires gap closing but without need of any symmetry breaking. Traditionally these phase transitions occur in macro-

scopic systems in condensed matter. Recently few-body quantum phase transition has received special attention [23–27, 56]. Various patterns of symmetry breaking can occur to induce tricriticalities and quadruple points even in a single-qubit system [28]. One may wonder whether there is any analog of topological phase transition in few-body systems.

In this work we study the anisotropic QRM to renew the understanding of the role of the counter-rotating term. Rather than conventional consideration of transitions in the low frequency limit, we shed light on the phase diagrams at finite frequencies, which enables us to illuminate an emerging structure of phase boundary series with gap closing. We find these emerging additional phase transitions are actually topological transitions without symmetry breaking. The number of zero points in the wave function turns out to be the topological number in the novel classification of the phases. We also find emerging series of multicriticalities beyond the conventional picture.

Model and symmetry.—The anisotropic QRM [22, 25] reads

$$H = \omega a^\dagger a + \frac{\Omega}{2} \sigma_x + g [(\tilde{\sigma}_- a^\dagger + \tilde{\sigma}_+ a) + \lambda (\tilde{\sigma}_+ a^\dagger + \tilde{\sigma}_- a)]$$

where $\sigma_{x,y,z}$ is the Pauli matrix, $a^\dagger(a)$ creates (annihilates) a bosonic mode with frequency ω . The coupling strength is denoted by g and the anisotropy by λ . The QRM is retrieved by $\lambda = 1$ and the JCM by $\lambda = 0$. By the transforms $a^\dagger = (\hat{x} - i\hat{p})/\sqrt{2}$, $a = (\hat{x} + i\hat{p})/\sqrt{2}$, $\hat{p} = -i\frac{\partial}{\partial x}$ and $\tilde{\sigma}^\pm = (\sigma_z \mp i\sigma_y)/2$, $\sigma_x = \sigma^+ + \sigma^-$, $\sigma_y = -i(\sigma_+ - \sigma_-)$ we can map to the effective spatial space

$$H = \frac{\omega}{2} \hat{p}^2 + v_{\sigma_z} + \left[\frac{\Omega}{2} - g_y i\sqrt{2}\hat{p}\right] \sigma^+ + \left[\frac{\Omega}{2} + g_y i\sqrt{2}\hat{p}\right] \sigma^- \quad (1)$$

where $g_y = \frac{(1-\lambda)}{2}g$, $g_z = \frac{(1+\lambda)}{2}g$ and $\varepsilon_0^y = -\frac{1}{2}[g_y'^2 + 1]\omega$. The harmonic potentials $v_{\sigma_z} = \omega(x + g_z'\sigma_z)^2/2 + \varepsilon_0^y$ in the two spin components are shifted in opposite directions by the coupling via $g_z' = \sqrt{2}g_y/\omega$. Then the Ω

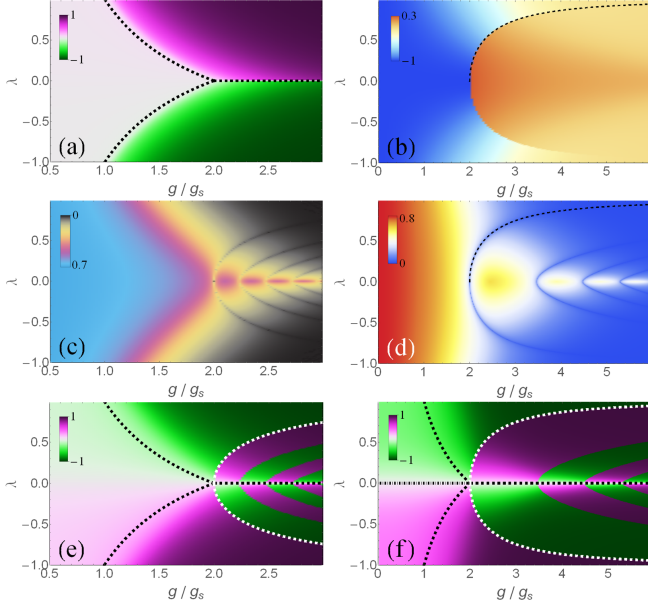


FIG. 1. (color online) *Multicriticality in phase diagrams of anisotropic QRM.* (a) $A = \langle a^\dagger a^\dagger \rangle / A_0$ of the ground state (GS) versus coupling g and anisotropy λ at $\omega = 0.01\Omega$. $A_0 = [(1 + |\lambda|)g / (2\omega)]^2$ (b) $\langle \sigma_x \rangle$ at $\omega = 2\Omega$. (c) First-excitation gap Δ at $\omega = 0.1\Omega$ (plotted by $\Delta^{1/6}$ to show the boundaries better). (d) $\Delta^{1/4}$ at $\omega = 0.5\Omega$. (e) $A * P$ at $\omega = 0.1\Omega$. P is parity. (f) $A * P$ at $\omega = 0.5\Omega$. The dashed lines in (a,b,d,e,d) are analytic boundaries.

term plays the role of spin flipping in spin $\sigma_z = \pm$ space and tunneling in the effective spatial space [26, 35]. The g_y term is Rashba spin-orbit coupling (RSOC) in competition with the Ω term. The model at any anisotropy possesses the parity symmetry $\hat{P} = \sigma_x (-1)^{a^\dagger a}$ which commutes with H [22].

Conventional phase diagram.—The anisotropic QRM has a quantum phase transition in the low frequency limit [25] at the transition boundary $g_c^\lambda = \frac{2}{1+|\lambda|}g_s$ where $g_s = \sqrt{\omega\Omega}/2$ is the transition point of the QRM. Above g_c^λ the ground states (GS) in positive and negative anisotropy are respectively x and p types, in the sense that the $\lambda > 0$ regime has finite expectation $\langle \hat{x}^2 \rangle$ but vanishing $\langle \hat{p}^2 \rangle$ while it is reversed in $\lambda < 0$ regime. So there are totally three phases. We can distinguish the three phases conveniently by one physical quantity $\langle a^\dagger a^\dagger \rangle$ which is equivalent to the difference of $\langle \hat{x}^2 \rangle$ and $\langle \hat{p}^2 \rangle$, as illustrated in Fig.1(a) by exact diagonalization at $\omega = 0.01\Omega$.

Excitation gap and novel phase diagram.— When we tune up the frequency we illuminate a fine structure of the phase diagram beyond the above conventional picture. In Fig.1(c) we show the map of the first excitation gap at $\omega = 0.1\Omega$, where one can see that, besides the conventional boundaries, there are a series of additional phase boundaries emerging. These boundaries show up in gap closing and reopening. These additional bound-

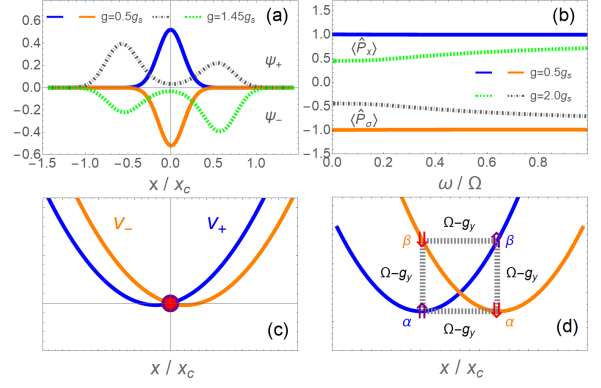


FIG. 2. (color online) *Hidden symmetry breaking at the transition g_c^λ .* (a) GS wave function ψ_\pm before (solid lines, $g = 0.5g_s$) and after transition (broken lines, $g = 1.45g_s$) at $\lambda = 0.5$ and $\omega = 0.01\Omega$. (b) $\langle \hat{P}_x \rangle$ and $\langle \hat{P}_y \rangle$ before and after transition. (c) Effective potential v_\pm before transition with dots marking the particle position. (d) v_\pm after transition. The arrows represent the spins and dashed lines label the tunneling (Ω) and RSOC coupling (g_y). α, β are wave-packet weights and $x_c = \sqrt{2}g_s/\omega$.

aries become sparser when we raise the frequency higher, as $\omega = 0.5\Omega$ in panel (d). Although higher boundaries are moving with the increase of frequency, the primary one of the additional boundaries remains invariant. Let us label the primary one by g_{T1} . It should be mentioned that, unlike the second-order transition g_c^λ , the additional phase transitions are of first order. This first order feature can be reflected in the spin expectation $\langle \sigma_x \rangle$ as shown by Fig.1(b) with $\omega = 2\Omega$, despite that the discontinuity decreases with the coupling strength.

Multicriticality.—The additional transition boundaries involves changes of parity P . We notice that the parity is symmetric with respect to JCM line at $\lambda = 0$ while the $\langle a^\dagger a^\dagger \rangle$ is antisymmetric. Combining the two quantities unveils a novel phase diagram as in Fig.1(e) with $\omega = 0.1\Omega$. We see that the conventional triple point becomes a quintuple point and the tricriticality becomes a pentacriticality. Moreover, following the pentacriticality a series of quadruple points and tetra-criticalities emerge. Raising the frequency higher, as $\omega = 0.5\Omega$ in Fig.1(f), the difference between the positive and negative λ regimes also arises for the weak couplings below g_c^λ . This is coming from the breaking of the U(1) symmetry, i.e. the excitation number $\hat{E} = a^\dagger a + \sigma_x$, which is a symmetry of the JCM. Thus, if taking this U(1)-breaking boundary into account, the novel pentacriticality would renew again to turn to be a hexacriticality.

Hidden symmetry breaking at transition g_c^λ .—Before revealing the nature of the additional series transitions, let us first re-visit the conventional transition g_c^λ to unveil its symmetry-breaking aspect. Although the anisotropic QRM possesses the parity symmetry overall the parameter regime, we find the transition g_c^λ also undergoes a

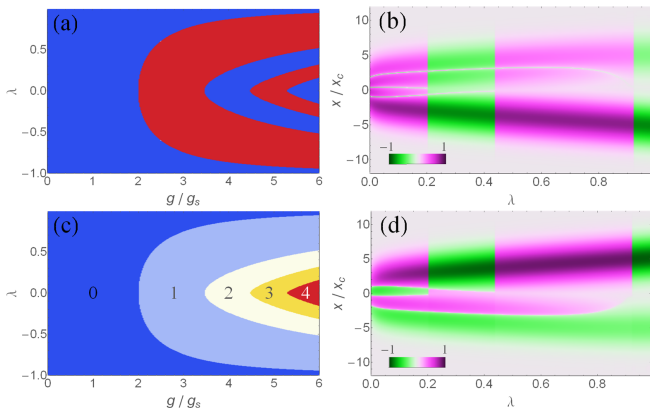


FIG. 3. (color online) *Parity and topological transitions.* (a) Phase diagram of the GS parity with $P = -1$ (blue) and $P = 1$ (red). (b) $\psi_+(x) * \psi_-(-x)$ versus λ at $g = 5.2g_s$. (c) Topological phase diagram. The numbers mark zero numbers n_z . (d) $\psi_-(x)$ versus λ . Here $\omega = 0.5$ and the color contrast in (b,d) is enhanced by amplified amplitude $|\psi_{\pm}|^{1/4}$.

symmetry breaking which is hidden. Let us decompose the parity into two parts, $\hat{P} = \hat{P}_\sigma \hat{P}_x$ where $\hat{P}_\sigma = \sigma_x$ reverses the spin while $\hat{P}_x = (-1)^{a^\dagger a}$ effectively inverts the spatial space $x \rightarrow -x$ [28]. For the general cases of the anisotropic QRM, both the spin reversion and the space inversion are needed to achieve the parity symmetry, while generally the model does not possess the individual symmetry of either \hat{P}_σ or \hat{P}_x . However, the GS before the transition g_c^λ is an exception.

In fact, in this regime the GS is a Gaussian-like wave packet in each spin component as shown by the solid lines in Fig.2(a). This is because, despite of the potential separation, in weak couplings the effective particle tends to stay at the origin to gain a maximum spin flipping or tunneling energy (Ω term), as sketched in Fig.2(c). The weak coupling g provides a small potential separation g'_z . The RSOC coupling (g_y term in Eq.(1)) not only depends on g but also cancels itself for the Gaussian wave packet at the origin. Thus the spin flipping is dominating before the transition g_c^λ . The degenerate potential at the origin gives an equal weight for the two spins, while a symmetric wave packet yields a maximum wave-packet overlap favorable for gaining more spin flipping energy. As a consequence, the state possesses both \hat{P}_x and \hat{P}_σ symmetries. After the transition the wave function splits into two packets, as shown in by the broken lines in Fig.2(a). As the packet weights on the two sides are imbalanced due to the potential difference as indicated in Fig.2(d), neither symmetry of \hat{P}_x and \hat{P}_σ can be preserved. Therefore the conventional transition at g_c^λ is accompanied with a hidden symmetry breaking of \hat{P}_σ and \hat{P}_x . Fig.2(b) shows the expectation of \hat{P}_σ and \hat{P}_x with amplitudes remaining at 1 before the transition indicating preserved symmetries and deviation from 1 after the transition meaning broken symmetries.

Topological phase transitions.—So far we have seen that the transitions at g_c^λ and at $\lambda = 0$ are all accompanied with some symmetry breaking. Now we look at the additional series transitions. Since the parity symmetry is valid for all parameter regimes, these additional transitions do not break the parity symmetry either. Indeed the parity changes the sign at these transitions, as shown by Fig.3(a). However, the parity has only two values, not enough to label the series phases separated by the additional transition boundaries. In fact, we find that the additional transitions are topological phase transitions which are different class of phase transition from those transitions at g_c^λ and at $\lambda = 0$. The phases separated by these topological transitions are distinguished from each other by their topological feature, each of them having an individual topological number.

Indeed, the wave function in each phase belt has a same number of zero points n_z . In Fig.3(b), we show the wave function by the product of the spin-up and spin-down components, $\psi_P(x) = \psi_+(x) * \psi_-(-x)$, in the variation of the anisotropy at a fixed coupling. Starting from the QRM side at $\lambda = 1$ we have $\psi_P(x)$ all non-negative (yellow) in x space, indicating the negative parity. Reducing the value of λ till the JCM side at $\lambda = 0$, we have three topological transitions. At each transition $\psi_P(x)$ changes between non-negative (yellow) and non-positive (blue), indicating a changeover between negative and positive parities. A closer look at the evolution of $\psi_P(x)$ in Fig.3(b), one can notice some white lines appearing. These white lines are actually zero-value lines. Each phase has a same n_z number, thus forming lines. From the QRM to the JCM we have zero line number $n_z=0, 1, 2, 3$ corresponding to the four phases. The zero lines can be more clearly visualized from $\psi_-(x)$ as in Fig.3(d), where the color shifts between yellow and blue if tracking along the x dimension. Given a fixed number n_z , one cannot go to another n_z state by continuous shape deformation of the wave function. Thus the zero number n_z is the topological number of each phase. We extract the topological phase diagram in Fig.3(c) where the numbers mark n_z . These topological phase transitions are accompanied with gap closing, as in Fig.1(d). The afore-discussed transition at g_c^λ occurs within the topological phase $n_z = 0$, without undergoing a topological transition in the wave-packet splitting. The gap at g_c^λ becomes small in lowering frequency, but never exactly closes unless $\omega = 0$.

Negative λ and x - p Duality.—The afore-discussed topological transition in x space refers to the $\lambda \geq 0$ regime. For the $\lambda < 0$ regime, the quantum state is p type as mentioned in the conventional phase diagram. Thus topological character should lie in the p space instead of the x space. Indeed by the spin rotation and x - p exchange $\{\sigma_x, \sigma_y, \sigma_z\} \rightarrow \{\sigma_x, -\sigma_z, \sigma_y\}$, $-i\partial_x \rightarrow p$, $x \rightarrow i\partial_p$ one can get the dual form of Hamiltonian (1) in the p space, with g_y and g_z exchange the roles as now λ is negative. In

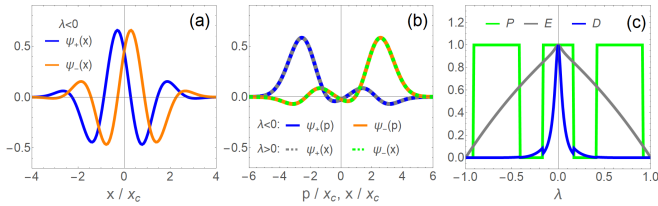


FIG. 4. (color online) *x-p duality and spontaneous symmetry breaking*. (a) Wave function in x space for $\lambda = -0.1$ (b) Wave function in p space for $\lambda = -0.1$ (solid) which coincides with that of $\lambda = 0.1$ (dashed) in x space. (c) Expectation of parity ($P = \langle \hat{P} \rangle$), plotted by $(P + 1)/2$, excitation number ($E = \langle \hat{n} + \sigma_x \rangle$), plotted by normalized $E(1) - E(\lambda)$ and x - p duality (D). Here we illustrate at $g = 5g_s$ and $\omega = 0.5\Omega$.

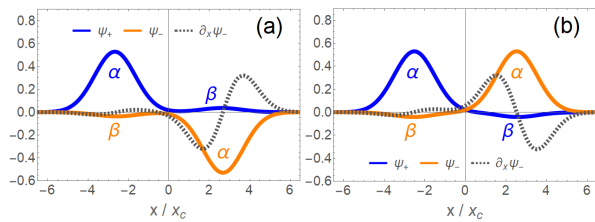


FIG. 5. (color online) *Energy competition around the primary topological transition*. ψ_{\pm} and $\partial_x \psi_{\pm}$ before (a) and after (b) the transition g_{T1} at $\lambda = 0.7, 0.8$ respectively. Here $g = 3.0g_s$ and $\omega = 0.5\omega$.

Fig.4(a) we illustrate the wave function in the x space for $\lambda < 0$, which seemingly does not match the topological feature extracted above. However as shown in Fig.4(b), after the mapping to the p space, the wave function exactly becomes the same as that in the x space from $\lambda > 0$ regime, up to an irrelevant total phase.

Spontaneous symmetry breaking (SSB).—The JCM is invariant under the above mapping as $g_y = g_z$ at $\lambda = 0$, and it is also easy to show analytically that the JCM wave function, which has a form $\psi_{n\pm}^{(z)} = C_n \phi_n \mp C_n \phi_{n+1}$ where ϕ_n is the quantum Harmonic oscillator, is invariant under the duality mapping. Let us denote such a duality symmetry by D . Thus the JCM has the parity symmetry P , the $U(1)$ symmetry (excitation number E) and the duality symmetry D . It is worth having a comparison of how these symmetries are affected by the anisotropy. Fig.4(c) we plot the expectations of the symmetry operations versus λ . In contrast to preserved P and mildly broken E , above g_c^λ there is a SSB behavior in D , sharper for lower frequencies and stronger couplings. Below g_c^λ (unplotted), the variation in E remains similar to above g_c^λ , while the sharp change of D is flattened and D even becomes unbroken in low frequency limit. Under the protection of parity, topological transition is however unaffected by the D -SSB, but triggered by gap closing.

Wave-function braiding and gap closing.—As afore-discussed, after the transition g_c^λ the GS wave function splits into two packets, which can be represented

by[26] $\psi_+(x) = \alpha\varphi_\alpha + \beta\varphi_\beta$ with weights α, β and $\psi_-(x) = -\psi_+(-x)$ under the parity symmetry. As sketched in Fig.2(d), there are four channels of tunneling and RSOC, i.e. $\Omega_{\gamma\gamma'} = -\frac{\Omega}{2} \gamma\gamma' \langle \varphi_\gamma(x) | \varphi_{\gamma'}(-x) \rangle$ and $g_{\gamma\gamma'}^y = \sqrt{2}g_y\gamma\gamma' \langle \varphi_\gamma(x) | \partial_x \varphi_{\gamma'}(-x) \rangle$ with $\gamma, \gamma' \in \{\alpha, \beta\}$, respectively. We see $\Omega_{\gamma\gamma'}$ and $g_{\gamma\gamma'}^y$ are counteracting. Starting from $\lambda = 1$ we know from the QRM side φ_α and φ_β can be approximated by a displaced harmonic oscillator, while α, β are positive to gain more negative tunneling energy[26]. Thus there is no zero point before g_{T1} . After g_{T1} there is one zero point in $\psi_{\sigma_z}(x)$ so that $\psi_{\sigma_z}(x)$ is braided once, which can be simply realized by changing the sign of α in ψ_- (not the sign of β otherwise the dominant same-side tunneling energy $\Omega_{\alpha\beta}$ becomes positive) and β in ψ_+ . Thus the main peak of ψ_- flips (orange in Fig.5(a,b)) and the parity is reversed. Under this wave-function braiding, the same-side energies $\Omega_{\alpha\beta}$ and $g_{\alpha\beta}^y$ are unaffected and the dominant competition comes from the opposite-side ones $\Omega_{\gamma\gamma'}, g_{\gamma\gamma'}^y$. The leading contributions together are $E_{\Omega y} = \Omega_{\alpha\alpha} + g_{\alpha\alpha}^y = \mp \alpha^2 (\frac{\Omega}{2} - \frac{2g_y g_z}{\omega}) \exp[-g_z'^2]$ and the sign \mp corresponds to before and after the transition. Note the opposite-side kinetic and potential terms are not competitive as their weight product $\alpha\beta$ from a same spin component is much smaller than α^2 in the large g . Setting $E_{\Omega y} = 0$ gives the transition boundary

$$g_{T1} = 2g_s/\sqrt{1-\lambda^2}, \quad \lambda_{T1} = \sqrt{1-4g_s/g^2} \quad (2)$$

which is frequency-independent and matches well with the numerics as in Fig.1. Further topological transitions similarly involve more wave-function braidings, each time occurs with the energy reversing, thus always associated with gap closing.

Conclusions.—By mapping to a RSOC model we have studied the phase transitions in the anisotropic QRM which connects the fundamental QRM and JCM. By turning on finite frequencies we have unveiled a novel phase diagram with a fine structure of phase boundary series in gap closing and reopening, which is beyond the conventional picture in the low frequency limit. The conventional transition is accompanied with a hidden symmetry breaking, whereas the emerging gap-closing transitions are topological transitions without symmetry breaking. We find the number of zero points in the wave function is the topological number. We see this topological feature provides a novel universality classification in bridging the QRM and the JCM, among the diversity arising from going away from the low frequency limit where there is a universality[25]. We have also shown that the conventionally established triple point is actually a quintuple or sextuple point and following the penta-/hexa-criticality emerge a series of tetra-criticalities. Our work demonstrates that a single-qubit system can exhibit multicriticalities and topological transitions.

Acknowledgements.—This work was supported by

the National Natural Science Foundation of China (Grant No. 11974151).

* yingzj@lzu.edu.cn

- [1] P. Forn-Díaz, L. Lamata, E. Rico, J. Kono, and E. Solano, *Rev. Mod. Phys.* **91**, 025005 (2019) and references therein.
- [2] A. Frisk Kockum, A. Miranowicz, S. De Liberato, S. Savasta, and F. Nori, *Nature Reviews Physics* **1**, 19 (2019).
- [3] D. Braak, *Phys. Rev. Lett.* **107**, 100401 (2011).
- [4] A. Le Boité, *Adv. Quantum Technol.* **3**, 1900140 (2020).
- [5] P. Forn-Díaz, J. Lisenfeld, D. Marcos, J. J. García-Ripoll, E. Solano, C. J. P. M. Harmans, and J. E. Mooij, *Phys. Rev. Lett.* **105**, 237001 (2010).
- [6] A. Wallraff, D. I. Schuster, A. Blais, L. Frunzio, R.-S. Huang, J. Majer, S. Kumar, S. M. Girvin, and R. J. Schoelkopf, *Nature* **431**, 162 (2004).
- [7] T. Niemczyk, F. Deppe, H. Huebl, E. P. Menzel, F. Hocke, M. J. Schwarz, J. J. García-Ripoll, D. Zueco, T. Hümmer, E. Solano, A. Marx, and R. Gross, *Nature Phys.* **6**, 772 (2010).
- [8] G. Günter, A. A. Anappara, J. Hees, A. Sell, G. Biasiol, L. Sorba, S. De Liberato, C. Ciuti, A. Tredicucci, A. Leitenstorfer and R. Huber, *Nature* **458**, 178 (2009).
- [9] P. Forn-Díaz, J. J. García-Ripoll, B. Peropadre, J. L. Orgiazzi, M. A. Yurtalan, R. Belyansky, C.M. Wilson, and A. Lupascu, *Nat. Phys.* **13**, 39 (2017).
- [10] B. Peropadre, P. Forn-Díaz, E. Solano, and J. J. García-Ripoll, *Phys. Rev. Lett.* **105**, 023601 (2010).
- [11] G. Scalari, C. Maissen, D. Turčinková, D. Hagenmüller, S. De Liberato, C. Ciuti, C. Reichl, D. Schuh, W. Wegscheider, M. Beck, and J. Faist, *Science* **335**, 1323 (2012).
- [12] F. Yoshihara, T. Fuse, S. Ashhab, K. Kakuyanagi, S. Saito, and K. Semba, *Nat. Phys.* **13**, 44 (2017).
- [13] Z.-L. Xiang, S. Ashhab, J. Q. You, and F. Nori, *Rev. Mod. Phys.* **85**, 623 (2013).
- [14] X. Gu, A. F. Kockum, A. Miranowicz, Y. X. Liu, F. Nori, *Phys. Rep.* **718**, 1 (2017).
- [15] F. A. Wolf, M. Kollar, and D. Braak, *Phys. Rev. A* **85**, 053817 (2012).
- [16] E. Solano, *Physics* **4**, 68 (2011).
- [17] S. Felicetti and A. Le Boité, *Phys. Rev. Lett.* **124**, 040404 (2020).
- [18] S. Felicetti, M.-J. Hwang, and A. Le Boité, *Phys. Rev. A* **98**, 053859 (2018).
- [19] S. Felicetti, D. Z. Rossatto, E. Rico, E. Solano, and P. Forn-Díaz, *Phys. Rev. A* **97**, 013851 (2018).
- [20] S. Felicetti, J. S. Pedernales, I. L. Egusquiza, G. Romero, L. Lamata, D. Braak, and E. Solano, *Phys. Rev. A* **92**, 033817 (2015).
- [21] H. P. Eckerle and H. Johannesson, *J. Phys. A: Math. Theor.* **50**, 294004 (2017).
- [22] Q.-T. Xie, S. Cui, J.-P. Cao, L. Amico, and H. Fan, *Phys. Rev. X* **4**, 021046 (2014).
- [23] S. Ashhab, *Phys. Rev. A* **87**, 013826 (2013).
- [24] M.-J. Hwang, R. Puebla, and M. B. Plenio, *Phys. Rev. Lett.* **115**, 180404 (2015).
- [25] M. Liu, S. Chesi, Z.-J. Ying, X. Chen, H.-G. Luo, and H.-Q. Lin, *Phys. Rev. Lett.* **119**, 220601 (2017).
- [26] Z.-J. Ying, M. Liu, H.-G. Luo, H.-Q. Lin and J. Q. You, *Phys. Rev. A* **92**, 053823 (2015).
- [27] Z.-J. Ying, L. Cong, and X.-M. Sun, arXiv:1804.08128 (2018); *J. Phys. A: Math. Theor.* **53**, 345301 (2020).
- [28] Z.-J. Ying, arXiv:2010.01379 (2020).
- [29] M. Liu, Z.-J. Ying, J.-H. An, and H.-G. Luo, *New J. Phys.* **17**, 043001 (2015).
- [30] L. Cong, X.-M. Sun, M. Liu, Z.-J. Ying, and H.-G. Luo, *Phys. Rev. A* **95**, 063803 (2017).
- [31] L. Cong, X.-M. Sun, M. Liu, Z.-J. Ying, and H.-G. Luo, *Phys. Rev. A* **99**, 013815 (2019).
- [32] Q.-H. Chen, C. Wang, S. He, T. Liu, and K.-L. Wang, *Phys. Rev. A* **86**, 023822 (2012).
- [33] L. Duan, Y.-F. Xie, D. Braak, and Q.-H. Chen, *J. Phys. A* **49**, 464002 (2016).
- [34] Z. Lü, C. Zhao, and H. Zheng, *J. Phys. A: Math. Theor.* **50**, 074002 (2017).
- [35] E. K. Irish and J. Gea-Banacloche, *Phys. Rev. B* **89**, 085421 (2014).
- [36] M. T. Batchelor and H.-Q. Zhou, *Phys. Rev. A* **91**, 053808 (2015).
- [37] Q. Xie, H. Zhong, M. T. Batchelor, and C. Lee, *J. Phys. A: Math. Theor.* **50**, 113001 (2017).
- [38] S. Bera, S. Florens, H. U. Baranger, N. Roch, A. Nazir, and A. W. Chin, *Phys. Rev. B* **89**, 121108(R) (2014).
- [39] L. Yu, S. Zhu, Q. Liang, G. Chen, and S. Jia, *Phys. Rev. A* **86**, 015803 (2012).
- [40] T. Liu, M. Feng, W. L. Yang, J. H. Zou, L. Li, Y. X. Fan, and K. L. Wang, *Phys. Rev. A* **88**, 013820 (2013).
- [41] Y.-Y. Zhang, *Phys. Rev. A* **94**, 063824 (2016).
- [42] L.-T. Shen, Z.-B. Yang, H.-Z. Wu, and S.-B. Zheng, *Phys. Rev. A* **95**, 013819 (2017).
- [43] J. Peng, E. Rico, J. Zhong, E. Solano, and I. L. Egusquiza, *Phys. Rev. A* **100**, 063820 (2019).
- [44] J. Casanova, R. Puebla, H. Moya-Cessa and M. B. Plenio, *npj Quantum Information* **4**, 47 (2018).
- [45] I. I. Rabi, *Phys. Rev.* **51**, 652 (1937).
- [46] E. T. Jaynes and F. W. Cummings, *Proc. IEEE* **51**, 89 (1963).
- [47] G. Romero, D. Ballester, Y. M. Wang, V. Scarani, and E. Solano, *Phys. Rev. Lett.* **108**, 120501 (2012).
- [48] I. Pietikäinen, S. Danilin, K. S. Kumar, A. Vepsäläinen, D. S. Golubev, J. Tuorila, and G. S. Paraoanu, *Phys. Rev. B* **96**, 020501(R) (2017).
- [49] Y. Wang, W.-L. You, M. Liu, Y.-L. Dong, H.-G. Luo, G. Romero, and J. Q. You, *New J. Phys.* **20**, 053061 (2018).
- [50] L. D. Landau, *Zh. Eksp. Teor. Fiz.* **7**, 19 (1937).
- [51] D. J. Thouless, M. Kohmoto, M. P. Nightingale, and M. den Nijs, *Phys. Rev. Lett.* **49**, 405 (1982).
- [52] J M Kosterlitz and D J Thouless. *Journal of Physics C: Solid State Phys.* **6**, 1181 (1973).
- [53] F.D.M. Haldane. *Phys. Lett. A* **93**, 464, (1983).
- [54] F.D.M. Haldane. *Phys. Rev. Lett.* **50**, 1153 (1983).
- [55] Z.-C. Gu and X.-G. Wen, *Phys. Rev. B* **80**, 155131 (1990).
- [56] H.-J. Zhu, K. Xu, G.-F. Zhang, and W.-M. Liu, *Phys. Rev. Lett.* **125**, 050402 (2020).